

# LFT modeling and mu-analysis of Darwin type spacecraft

***Citation for published version (APA):***

Denie, D. S. M. (2007). *LFT modeling and mu-analysis of Darwin type spacecraft*. (DCT rapporten; Vol. 2007.013). Technische Universiteit Eindhoven.

***Document status and date:***

Published: 01/01/2007

***Document Version:***

Publisher's PDF, also known as Version of Record (includes final page, issue and volume numbers)

***Please check the document version of this publication:***

- A submitted manuscript is the version of the article upon submission and before peer-review. There can be important differences between the submitted version and the official published version of record. People interested in the research are advised to contact the author for the final version of the publication, or visit the DOI to the publisher's website.
- The final author version and the galley proof are versions of the publication after peer review.
- The final published version features the final layout of the paper including the volume, issue and page numbers.

[Link to publication](#)

***General rights***

Copyright and moral rights for the publications made accessible in the public portal are retained by the authors and/or other copyright owners and it is a condition of accessing publications that users recognise and abide by the legal requirements associated with these rights.

- Users may download and print one copy of any publication from the public portal for the purpose of private study or research.
- You may not further distribute the material or use it for any profit-making activity or commercial gain
- You may freely distribute the URL identifying the publication in the public portal.

If the publication is distributed under the terms of Article 25fa of the Dutch Copyright Act, indicated by the "Taverne" license above, please follow below link for the End User Agreement:

[www.tue.nl/taverne](http://www.tue.nl/taverne)

***Take down policy***

If you believe that this document breaches copyright please contact us at:

[openaccess@tue.nl](mailto:openaccess@tue.nl)

providing details and we will investigate your claim.

# LFT modeling and $\mu$ -analysis of Darwin type spacecraft

D.S.M. Denie

DCT 2007.013

Traineeship report

Supervisor: prof.dr.ir. Maarten Steinbuch

Technische Universiteit Eindhoven  
Department Mechanical Engineering  
Dynamics and Control Technology Group

Eindhoven, February, 2007



# Contents

<b>1</b>	<b>Introduction</b>	<b>3</b>
<b>2</b>	<b>The analytical model of the satellite</b>	<b>5</b>
2.1	Mass matrix . . . . .	5
2.2	Modal matrix . . . . .	6
2.3	State space representation . . . . .	8
<b>3</b>	<b>Uncertainty Modeling of satellite</b>	<b>9</b>
3.1	Uncertainty modeling using LFT . . . . .	9
3.1.1	LFT modeling of satellite mass and inertia . . . . .	10
3.1.2	LFT modeling of stiffness and damping . . . . .	11
3.1.3	LFT modeling of the beam mass . . . . .	14
3.1.4	LFT modeling of total plant . . . . .	14
3.2	Rearrange the $\Delta$ -block . . . . .	14
3.3	Verification of LFT model . . . . .	15
<b>4</b>	<b><math>\mu</math>-analysis</b>	<b>17</b>
4.1	$\mu$ -analysis of all parameters separately . . . . .	17
4.2	Model satellite with pulsation uncertain . . . . .	19
4.3	$\mu$ -analysis pulsation uncertain . . . . .	19
4.4	Worst case $\Delta$ for pulsation uncertain . . . . .	20
4.5	Time domain plot of pulsation worst case . . . . .	21
4.6	Symmetric property of satellite plant . . . . .	23
4.7	Applying $\Delta$ reduction . . . . .	24
<b>5</b>	<b>Conclusion</b>	<b>25</b>

<i>CONTENTS</i>	1
<b>A Standard operations on LFTs</b>	27
<b>B mussv algorithm</b>	29
<b>C Bode diagram of MIMO QFT controller</b>	33
<b>Bibliography</b>	34



# Chapter 1

## Introduction

The objective of this study is to analyze the robust stability of a MIMO QFT controller, applied as (negative) feedback on a satellite. The mission that has been chosen as a reference is the Scientific satellite Darwin. The Darwin Satellite corresponds to an ESA cornerstone mission, scheduled for launch in the 2014 timeframe. The objective of the mission is to find Earth-like planets orbiting nearby stars and analyzing their atmosphere through appropriate spectroscopy techniques to detect signs of life.

For detecting such faint objects as planets orbiting around their sun, Darwin relies upon nulling interferometry: the light collected by six free flying telescopes is recombined inside a central 'hub', in a way that the beams from the star interfere destructively, while those from the planet interfere constructively.

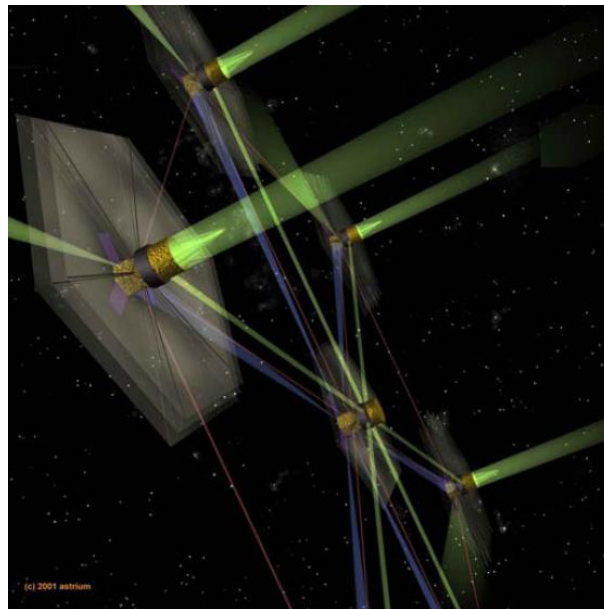


Figure 1.1: Interferometer constellation, 6 satellites (flyers) + 1 Hub

In the frame of the Large flimsy appendages control study [2], we limit the control synthesis to a unique satellite, i.e. corresponding to one of the flyer of the constellation. We consider the requirement in terms of position and attitude directly in terms of requirements applied to the single flyer and

not for the constellation as a whole. We are interested in the coupling between the satellite dynamics and the Flyer large sun-shield dynamics. In order to protect the instrument from the sunlight, all the flyers are equipped with large sun-shield, which are modeled with 6 large flexible booms.

From earlier studies an analytical model is available, which represents the unique satellite and the mentioned MIMO QFT controller. To analyze the robust stability of the satellite with the feedback MIMO QFT controller, we first model the uncertainty of the satellite using Linear Fractional Transformation (LFT) techniques. Then the mu-analysis is applied to investigate the robust stability and we would also like to calculate the worst case values of the uncertain parameters.

In chapter 2 the satellite model is presented, without uncertainties. Then, the mentioned uncertainty modeling is applied in chapter 3. Chapter 4 will discuss the mu-analysis and is followed by some conclusions in chapter 5.



## Chapter 2

# The analytical model of the satellite

The analytical model of the satellite is determined in [2]. In this chapter the model is explained in short for completeness. The model consists of one rigid body with a number of flexible appendages (beams) attached to it. In total there are 6 beams considered (see figure 2.1). In order to calculate the dynamical model of the satellite, the first step consists in calculating the mass matrix of the whole structure. Next the modal participation matrix is calculated and the flexible modes of the beams are determined. These pulsations are used to find the stiffness and damping matrix. The resulting state space representation follows from these matrices.

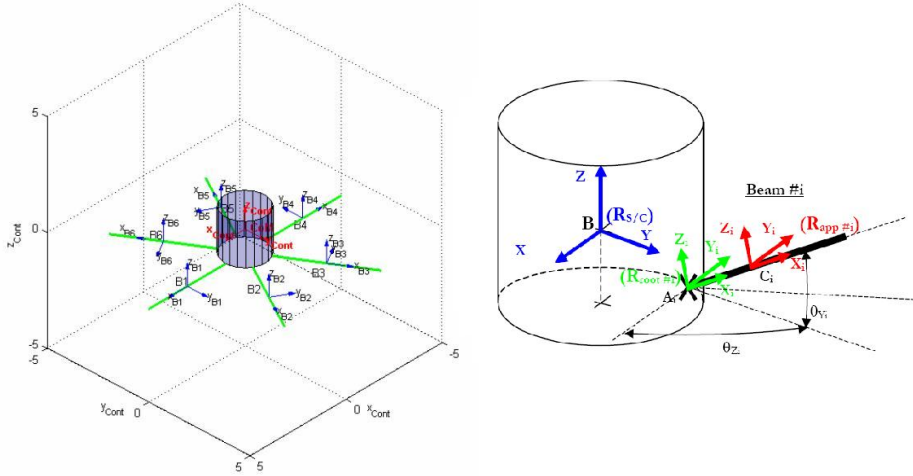


Figure 2.1: Model of satellite with beams

## 2.1 Mass matrix

The mass matrix is calculated as the sum of the mass of the rigid body and the mass matrix of the beams, expressed within the same frame. This boils down to:

$$M(6 \times 6)_{tot}|_{R_{sat}} = M(6 \times 6)_{rigidBody}|_{R_{sat}} + M(6 \times 6)_{beams}|_{R_{sat}} \quad (2.1)$$

where  $M(6 \times 6)_{rigidBody}|_{R_{sat}}$  is a diagonal matrix with on it's first three terms the rigid body mass and on the last three terms the rigid body inertia.  $M(6 \times 6)_{beams}|_{R_{sat}}$  follows from the sum of the mass and inertia of each beam, defined in the satellite frame, where the mass matrix of each (cylindric) beam is modeled in it's center of mass as:

$$M|_{beamCoM} = \begin{bmatrix} m_{app} & 0 & 0 & & \cdots & & 0 \\ 0 & m_{app} & 0 & & & & \\ 0 & 0 & m_{app} & 0 & & \ddots & \vdots \\ \vdots & \ddots & 0 & \frac{m \cdot R^2}{2} & 0 & & 0 \\ 0 & & \cdots & 0 & \frac{m}{12}(L^2 + 3R^2) & 0 & 0 \\ & & & & 0 & & \frac{m}{12}(L^2 + 3R^2) \end{bmatrix}$$

The mass matrices of each beam is then rotated and translated into the satellite frame. This rotation is achieved using the following formula (were  $i$  represents the beam number):

$$[M_i]_{satFrame}|_{(beamCoM)} = \begin{bmatrix} P_{i,R_{sat}/R_{beam}} & 0 \\ 0 & P_{i,R_{sat}/R_{beam}} \end{bmatrix}^T [M_i]_{beamFrame}|_{(beamCoM)} \begin{bmatrix} P_{i,R_{sat}/R_{beam}} & 0 \\ 0 & P_{i,R_{sat}/R_{beam}} \end{bmatrix}$$

In this formula  $P_{i,R_{sat}/R_{beam}}$  is determined using:

$$P_{i,R_{sat}/R_{beam}} = \begin{bmatrix} \cos \theta_{Y_i} & 0 & -\sin \theta_{Y_i} \\ 0 & 1 & 0 \\ \sin \theta_{Y_i} & 0 & \cos \theta_{Y_i} \end{bmatrix} \begin{bmatrix} \cos \theta_{Z_i} & \sin \theta_{Z_i} & 0 \\ -\sin \theta_{Z_i} & \cos \theta_{Z_i} & 0 \\ 0 & 0 & 1 \end{bmatrix}$$

When this rotation is performed, the translation of the frame is done with:

$$[M_i]_{satFrame}|_{(satCoM)} = \Delta_{mass\_i}^T \cdot [M_i]_{satFrame}|_{(beamCoM)} \cdot \Delta_{mass\_i}$$

Here the translation matrix  $\Delta_{mass\_i}$  is:

$$\Delta_{mass\_i} = \begin{bmatrix} 1 & 0 & 0 & 0 & -(Z_B - Z_{C_i}) & (Y_B - Y_{C_i}) \\ 0 & 1 & 0 & (Z_B - Z_{C_i}) & 0 & -(X_B - X_{C_i}) \\ 0 & 0 & 1 & -(Y_B - Y_{C_i}) & (X_B - X_{C_i}) & 0 \\ 0 & 0 & 0 & 1 & 0 & 0 \\ 0 & 0 & 0 & 0 & 1 & 0 \\ 0 & 0 & 0 & 0 & 0 & 1 \end{bmatrix}$$

And hence, the mass matrix of each beam is expressed in the satellite frame. Now all these beam mass matrices can be summed up with the rigid body mass matrix according to (2.1). In the later, the beam mass is set to  $7[kg]$  and the satellite mass and inertia is set to  $500[kg]$  and  $250[kg \ m^2]$  respectively.

## 2.2 Modal matrix

Each beam is modeled with flexible modes. These modes can be calculated using:

$$\omega_k = \frac{\lambda_k^2}{\lambda_1^2} \begin{bmatrix} \omega_{Y1} \\ \omega_{Z1} \end{bmatrix}$$

Where  $\omega_{Y1}$  and  $\omega_{Z1}$  are defined as the 1st pulsations in Y and Z direction respectively and  $\lambda_k$  is listed in table 2.1. Thus for each beams the number of modeled modes can be chosen.

Mode k	1	2	3	4	$\geq 5$
$\lambda_k$	1.8751	4.6941	7.8548	10.996	$\frac{(2k-1)\pi}{2}$

Table 2.1:  $\lambda_k$  for each pulsation

The modal participation matrix is then calculated at each beam root using the following formulas:

$$L_i|_{BeamRoot} = \begin{bmatrix} L_{TX1} & L_{TY1} & L_{TZ1} & L_{RX1} & L_{RY1} & L_{RZ1} \\ \vdots & \vdots & \vdots & \vdots & \vdots & \vdots \\ L_{TXN_{mode}} & L_{TYN_{mode}} & L_{TZN_{mode}} & L_{RXN_{mode}} & L_{RYN_{mode}} & L_{RZN_{mode}} \end{bmatrix}$$

$$= \begin{bmatrix} 0 & 2\sqrt{m}\frac{c_1}{\lambda_1} & 0 & 0 & 0 & 2\frac{\sqrt{m}L}{\lambda_1^2} \\ 0 & 0 & 2\sqrt{m}\frac{c_1}{\lambda_1} & 0 & -2\frac{\sqrt{m}L}{\lambda_1^2} & 0 \\ \vdots & \vdots & \vdots & \vdots & \vdots & \vdots \\ 0 & 2\sqrt{m}\frac{c_k}{\lambda_k} & 0 & 0 & 0 & 2\frac{\sqrt{m}L}{\lambda_k^2} \\ 0 & 0 & 2\sqrt{m}\frac{c_k}{\lambda_k} & 0 & -2\frac{\sqrt{m}L}{\lambda_k^2} & 0 \end{bmatrix}$$

Here  $c_k = \frac{-\sin \lambda_k + \sinh \lambda_k}{\cos \lambda_k + \cosh \lambda_k}$  and  $k$  is the mode number. The odd numbered rows are devoted to de partition of the modes in the  $Y$ -direction ( $\omega_Y$ ), while the even numbered rows reflects the influence of the  $Z$ -direction ( $\omega_Z$ ). The modal matrix for each beam is then rotated and translated into the satellite frame, where they form the total modal matrix:

$$[L_{total}|_{satFrame}]_{(satCoM)} = \begin{bmatrix} [L_1|_{satFrame}]_{(satCoM)} \\ \vdots \\ [L_n|_{satFrame}]_{(satCoM)} \end{bmatrix}$$

The rotation of the modal matrix is performed with the following formula:

$$[L_i|_{satFrame}]_{(beamRoot)} = [L_i|_{beamFrame}]_{(beamRoot)} \begin{bmatrix} P_{i,R_{sat}/R_{beam}} & 0 \\ 0 & P_{i,R_{sat}/R_{beam}} \end{bmatrix}$$

Where the transformation matrix from satellite frame to beamnumber  $i$ -frame ( $P_{i,R_{sat}/R_{beam}}$ ) is calculated with:

$$P_{i,R_{sat}/R_{beam}} = \begin{bmatrix} \cos \theta_{Yi} & 0 & -\sin \theta_{Yi} \\ 0 & 1 & 0 \\ \sin \theta_{Yi} & 0 & \cos \theta_{Yi} \end{bmatrix} \begin{bmatrix} \cos \theta_{Zi} & \sin \theta_{Zi} & 0 \\ -\sin \theta_{Zi} & \cos \theta_{Zi} & 0 \\ 0 & 0 & 1 \end{bmatrix}$$

The translation of the modal matrix into the satellite frame is done with:

$$[L_i|_{satFrame}]_{(satCoM)} = [L_i|_{satFrame}]_{(beamRoot)} \Delta_{modal_i}$$

And the transformation matrix  $\Delta_{modal_i}$  to calculating the translation of the modal matrix from beam-number  $i$  root to the satellite frame origin is defined as:

$$\Delta_{modal_i} = \begin{bmatrix} 1 & 0 & 0 & 0 & -(Z_B - Z_{A_i}) & (Y_B - Y_{A_i}) \\ 0 & 1 & 0 & (Z_B - Z_{A_i}) & 0 & -(X_B - X_{A_i}) \\ 0 & 0 & 1 & -(Y_B - Y_{A_i}) & (X_B - X_{A_i}) & 0 \\ 0 & 0 & 0 & 1 & 0 & 0 \\ 0 & 0 & 0 & 0 & 1 & 0 \\ 0 & 0 & 0 & 0 & 0 & 1 \end{bmatrix}$$

### 2.3 State space representation

All the previously mentioned matrices resulted in a state space representation of the satellite dynamics. How this representation is derived from the differential equations is not shown here, only the state space is given:

$$\begin{aligned}\dot{x} &= Ax + Bu \\ y &= Cx + Du\end{aligned}$$

with:

$$A = \begin{bmatrix} M & 0 & L^T \\ 0 & I & 0 \\ L & 0 & I \end{bmatrix}^{-1} \begin{bmatrix} 0 & 0 & 0 \\ 0 & 0 & I \\ 0 & -\omega^2 & -2\xi\omega \end{bmatrix} \quad B = \begin{bmatrix} M & 0 & L^T \\ 0 & I & 0 \\ L & 0 & I \end{bmatrix}^{-1} \begin{bmatrix} I & 0 \\ 0 & I \\ 0 & 0 \end{bmatrix}$$

$$C = \begin{bmatrix} I & 0 & 0 \\ 0 & I & 0 \end{bmatrix} \quad D = \begin{bmatrix} 0 & 0 \\ 0 & 0 \end{bmatrix}$$

Here  $x = [V, \dot{\theta}, \eta, \dot{\eta}]^T$ , with  $V$  the velocity,  $\dot{\theta}$  the angle rate,  $\eta$  the modal coordinate and  $\dot{\eta}$  its derivative. The input consist of the force and torque, i.e.  $u = [F, T]$ . The output corresponds to the velocity and the angular rate, as can be concluded from the state space representation. Thus, if we should consider a satellite with 6 beams, each beam modeled with 2 modes, then the resulting model has 54 states. Because the  $L$  and  $I$  matrices have the size equal to 24 (2 modes in 2 directions for 6 beams), added the size of the  $M$  matrix (6). To complete the dynamical modeling of the satellite, the state space representation is integrated ones (multiplied with  $\frac{1}{s}$ ) and hence, this results in a model with 60 states.

## Chapter 3

# Uncertainty Modeling of satellite

In the model mentioned in chapter 2 there are some parameters considered uncertain and some are known. The uncertain parameters are summed up in table 3.1. Because the parameters suppose to lie in an interval, the maximum and minimum values or the uncertainty range in percentage of these parameters are given. The rest of the parameters, like the rigid body dimensions for example, are calculated or given and thus in the formulas replaced with constant values.

Parameter	minimum	maximum	%
mass	-	-	5
inertia	-	-	5
$\omega_1$	0.05 [Hz]	0.5[Hz]	-
$\xi$	0.1 [%]	1 [%]	-

Table 3.1: Uncertainty parameters of the satellite

In this chapter the modeling of the uncertainty parameters is presented using the Linear Fractional Transformation (LFT).

### 3.1 Uncertainty modeling using LFT

Modeling the uncertainty using LFT boils down to separation of the uncertain parameters from a nominal plant. The uncertainty is "pulled out" from the nominal plant and considered as virtual input as described in [5]. This theory is used in combination with some standard operations on LFTs, as described in [3], to model the uncertainty of the satellite. For the completeness the used operations in this report are summed up in Appendix A.

Using LFT, the varying parameters are first to be written in nominal values and deviation of these nominal values. The following equations can be used to do so.

$$\bar{p} = \frac{p_{max} + p_{min}}{2} \quad p_{\delta} = \frac{p_{max} - p_{min}}{2} \quad (3.1)$$

When the deviation of a variable is defined in percents, this value can first be rewritten in a maximal and minimal and than the above formulas can be used.

### 3.1.1 LFT modeling of satellite mass and inertia

First the modeling of the satellite mass ( $m_{sat}$ ) and the satellite inertia ( $i_{sat}$ ) are modeled in LFT. When the uncertainty is written in nominal values and the deviations as shown in equation (3.1), we can form the LFTs according to figure 3.1.

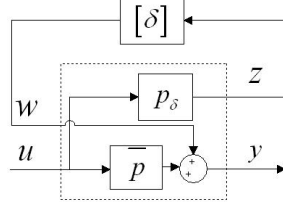


Figure 3.1: LFT of single parameter

From this we find the formulas to determine the general LFT for one uncertainty parameter. The formulas are:

$$\begin{bmatrix} z \\ y \end{bmatrix} = \begin{bmatrix} M_{11} & M_{12} \\ M_{21} & M_{22} \end{bmatrix} \begin{bmatrix} w \\ u \end{bmatrix} = \begin{bmatrix} 0 & p_\delta \\ 1 & \bar{p} \end{bmatrix} \begin{bmatrix} w \\ u \end{bmatrix}$$

$$w = \delta z$$

Making use of the juxtaposition standard operations on LFT (see appendix A) we can then define the LFT to model the satellites' mass and inertia uncertainties.

$$M_{11,sat} = \begin{bmatrix} 0 & 0 & 0 & 0 & 0 & 0 \\ 0 & 0 & 0 & 0 & 0 & 0 \\ 0 & 0 & 0 & 0 & 0 & 0 \\ 0 & 0 & 0 & 0 & 0 & 0 \\ 0 & 0 & 0 & 0 & 0 & 0 \\ 0 & 0 & 0 & 0 & 0 & 0 \end{bmatrix} \quad M_{12,sat} = \begin{bmatrix} m_{\delta,sat} & 0 & 0 & 0 & 0 & 0 \\ 0 & m_{\delta,sat} & 0 & 0 & 0 & 0 \\ 0 & 0 & m_{\delta,sat} & 0 & 0 & 0 \\ 0 & 0 & 0 & i_{\delta,sat} & 0 & 0 \\ 0 & 0 & 0 & 0 & i_{\delta,sat} & 0 \\ 0 & 0 & 0 & 0 & 0 & i_{\delta,sat} \end{bmatrix}$$

$$M_{21,sat} = \begin{bmatrix} 1 & 0 & 0 & 0 & 0 & 0 \\ 0 & 1 & 0 & 0 & 0 & 0 \\ 0 & 0 & 1 & 0 & 0 & 0 \\ 0 & 0 & 0 & 1 & 0 & 0 \\ 0 & 0 & 0 & 0 & 1 & 0 \\ 0 & 0 & 0 & 0 & 0 & 1 \end{bmatrix} \quad M_{22,sat} = \begin{bmatrix} \bar{m}_{sat} & 0 & 0 & 0 & 0 & 0 \\ 0 & \bar{m}_{sat} & 0 & 0 & 0 & 0 \\ 0 & 0 & \bar{m}_{sat} & 0 & 0 & 0 \\ 0 & 0 & 0 & \bar{i}_{sat} & 0 & 0 \\ 0 & 0 & 0 & 0 & \bar{i}_{sat} & 0 \\ 0 & 0 & 0 & 0 & 0 & \bar{i}_{sat} \end{bmatrix}$$

$$\Delta = \begin{bmatrix} \delta_1 I_{3 \times 3} & 0 \\ 0 & \delta_2 I_{3 \times 3} \end{bmatrix}$$

When this LFT is derived we end up with:

$$\begin{aligned} \mathcal{F}_u(M_{sat}, \Delta_{sat}) &= M_{22,sat} + M_{21,sat} (I - \Delta_{sat} M_{11,sat})^{-1} \Delta_{sat} M_{12,sat} \\ &= \begin{bmatrix} (\bar{m}_{sat} + \delta_1 m_{\delta,sat}) & 0 \\ 0 & (\bar{i}_{sat} + \delta_2 i_{\delta,sat}) I_{3 \times 3} \end{bmatrix} \end{aligned}$$

And hence, this is how the satellite mass occurs in the earlier determined mass matrix in section 2.1.

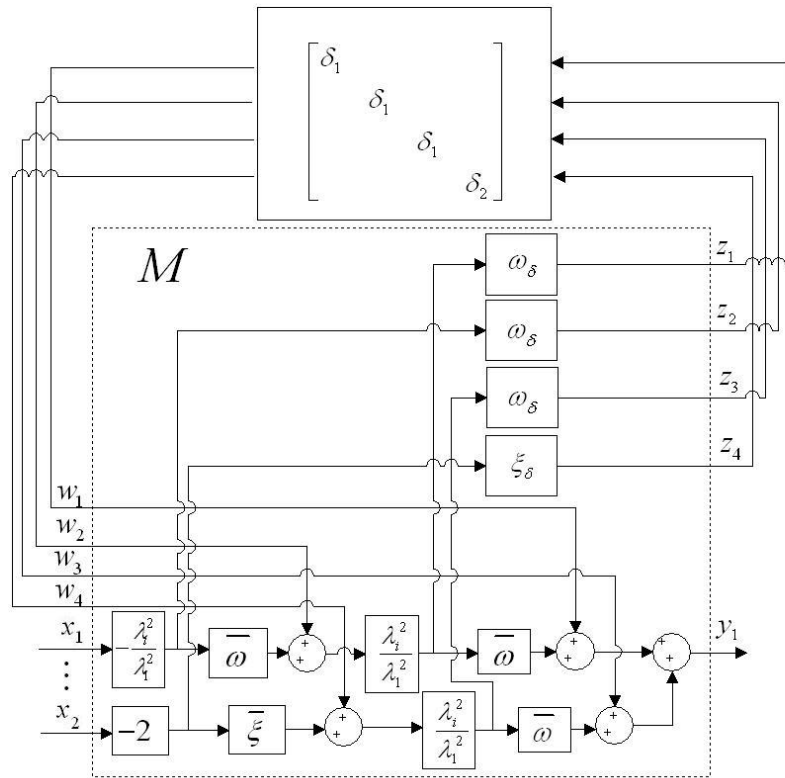
### 3.1.2 LFT modeling of stiffness and damping

Next, the modeling of the damping  $\xi$  and pulsation  $\omega$  for each beam and each mode in one direction is achieved. In the  $A$ -matrix these variables occur as (see section 2.3):

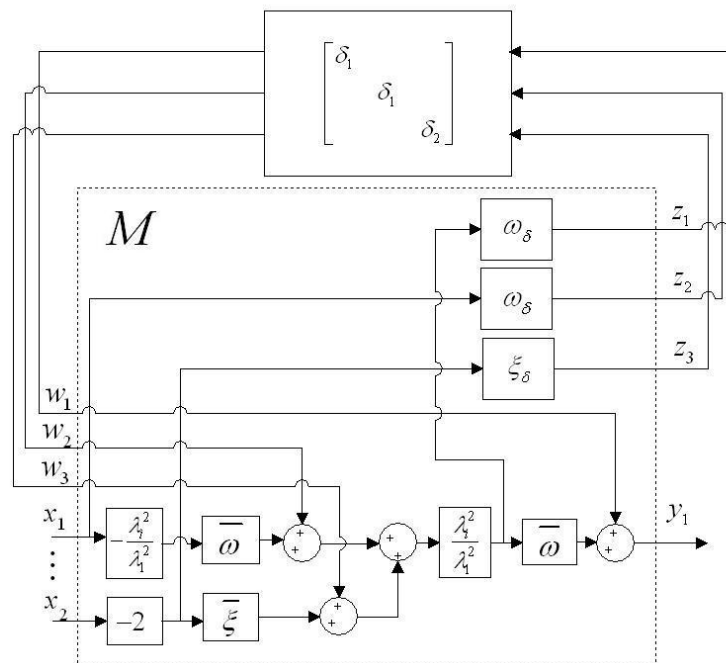
$$\left[ -\left(\frac{\lambda_i^2}{\lambda_1^2}(\bar{\omega} + \delta_1\omega_\delta)\right)^2 \quad 0 \quad \dots \quad 0 \quad -2\frac{\lambda_i^2}{\lambda_1^2}(\bar{\xi} + \delta_2\xi_\delta)(\bar{\omega} + \delta_1\omega_\delta) \right]$$

By taking these two uncertainties in one LFT, we can reduce the size of the  $\Delta$ -block. To show this, we shall present two LFT's, were in the first case we model the damping and stiffness matrix separately and in the second case we model them together.

In figure 3.2 the two different ways of modeling the damping and stiffness matrices are shown. We immediately see that modeling the two matrices apart (figure 3.2a) results in a larger  $\Delta$ -block. So there are more LFT models that represent the same uncertainty and the way uncertainty is modeled can influence the complexity of the problem. Fortunately there is a reduction method described in [3] that filters out the uncontrollable and unobservable parts of the  $\Delta$ -block. Using this method it is possible to reduce the size of the  $\Delta$  in figure 3.2a to that of figure 3.2b. Thus although we will use the LFT of figure 3.2b to model the damping and stiffness, in the later we will not concern ourself about obtaining the minimal LFT form when modeling the other uncertainties of table 3.1.



(a) Modeled separately



(b) Modeled together

Figure 3.2: LFT block diagram of stiffness and damping matrix



From figure 3.2b we obtain the following equations:

$$\begin{bmatrix} z_1 \\ z_2 \\ z_3 \\ y_1 \end{bmatrix} = \left[ \begin{array}{ccc|cc} 0 & a \omega_\delta & a \omega_\delta & -a^2 \bar{\omega} \omega_\delta & -2a \bar{\xi} \omega_\delta \\ 0 & 0 & 0 & -a \omega_\delta & 0 \\ 0 & 0 & 0 & 0 & -2\xi_\delta \\ \hline 1 & a \bar{\omega} & a \bar{\omega} & -(a \bar{\omega})^2 & -2a \bar{\xi} \bar{\omega} \end{array} \right] \begin{bmatrix} w_1 \\ w_2 \\ w_3 \\ x_1 \\ x_2 \end{bmatrix}$$

$$\begin{bmatrix} w_1 \\ w_2 \\ w_3 \end{bmatrix} = \begin{bmatrix} d_1 & 0 & 0 \\ 0 & d_1 & 0 \\ 0 & 0 & d_2 \end{bmatrix} \begin{bmatrix} z_1 \\ z_2 \\ z_3 \end{bmatrix}$$

In this formula  $a = \frac{\lambda_k^2}{\lambda_1^2}$ , while  $k$  represents the number of mode. Using these formulas, the LFT representation of one pulsation and one damping uncertain is already realized and we easily find the  $M$  and  $\Delta$ :

$$\mathcal{F}_u(M, \Delta) = \left( \left[ \begin{array}{ccc|cc} 0 & a \omega_\delta & a \omega_\delta & -a^2 \bar{\omega} \omega_\delta & -2a \bar{\xi} \omega_\delta \\ 0 & 0 & 0 & -a \omega_\delta & 0 \\ 0 & 0 & 0 & 0 & -2\xi_\delta \\ \hline 1 & a \bar{\omega} & a \bar{\omega} & -(a \bar{\omega})^2 & -2a \bar{\xi} \bar{\omega} \end{array} \right], \begin{bmatrix} \delta_1 I_{2 \times 2} & 0 \\ 0 & \delta_2 \end{bmatrix} \right) \quad (3.2)$$

When calculating this LFT, it boils down to:

$$\mathcal{F}_u(M, \Delta) = [ -a^2(\bar{\omega} + \delta_1 \omega_\delta) \quad -2a(\bar{\xi} + \delta_2 \xi_\delta)(\bar{\omega} + \delta_1 \omega_\delta) ]$$

Hence, this LFT results in a part of the damping and stiffness matrix. Another way to find this damping and stiffness LFT is to use the standard operations on LFT on the uncertainty parameters  $\omega$  and  $\xi$ . In this case a horizontal concatenation of the LFT's of  $\omega$  and  $\xi$  followed by a multiplication with the LFT of  $\omega$  would do. The advantage of using the standard operations is that they can be used to easily extend the number of uncertainties to represent the whole stiffness and damping matrix. For example, we can add the uncertainty of the  $\omega$  and  $\xi$  in the  $Z$ -direction to represent the uncertainty of one beam with one mode. This is done by applying juxtaposition on the  $\omega$  and  $\xi$ , which results in a total  $M$  and  $\Delta$ :

$$M = \left[ \begin{array}{cccccc|cccc} 0 & 0 & a \omega_\delta & 0 & a \omega_\delta & 0 & -a^2 \bar{\omega} \omega_\delta & 0 & -2a \bar{\xi} \omega_\delta & 0 \\ 0 & 0 & 0 & a \omega_\delta & 0 & a \omega_\delta & 0 & -a^2 \bar{\omega} \omega_\delta & 0 & -2a \bar{\xi} \omega_\delta \\ 0 & 0 & 0 & 0 & 0 & 0 & -a \omega_\delta & 0 & 0 & 0 \\ 0 & 0 & 0 & 0 & 0 & 0 & 0 & -a \omega_\delta & 0 & 0 \\ 0 & 0 & 0 & 0 & 0 & 0 & 0 & 0 & -2\xi_\delta & 0 \\ 0 & 0 & 0 & 0 & 0 & 0 & 0 & 0 & 0 & -2\xi_\delta \\ \hline 1 & 0 & a \bar{\omega} & 0 & a \bar{\omega} & 0 & -(a \bar{\omega})^2 & 0 & -2a \bar{\xi} \bar{\omega} & 0 \\ 0 & 1 & 0 & a \bar{\omega} & 0 & a \bar{\omega} & 0 & -(a \bar{\omega})^2 & 0 & -2a \bar{\xi} \bar{\omega} \end{array} \right] \quad (3.3)$$

$$\Delta = \begin{bmatrix} \delta_1 & 0 & 0 & 0 & 0 & 0 \\ 0 & \delta_2 & 0 & 0 & 0 & 0 \\ 0 & 0 & \delta_1 & 0 & 0 & 0 \\ 0 & 0 & 0 & \delta_2 & 0 & 0 \\ 0 & 0 & 0 & 0 & \delta_3 & 0 \\ 0 & 0 & 0 & 0 & 0 & \delta_4 \end{bmatrix}$$

Calculating this upper LFT as before results in:

$$\mathcal{F}_u(M, \Delta) = \begin{bmatrix} -a^2(\bar{\omega} + \delta_1 \omega_\delta)^2 & 0 & -2a(\bar{\xi} + \delta_3 \xi_\delta)(\bar{\omega} + \delta_1 \omega_\delta) & 0 \\ 0 & -a^2(\bar{\omega} + \delta_2 \omega_\delta)^2 & 0 & -2a(\bar{\xi} + \delta_4 \xi_\delta)(\bar{\omega} + \delta_2 \omega_\delta) \end{bmatrix}$$

Naturally it is more convenient to model the LFT using the standard operations instead of drawing a block diagram and determine the formulas from it, especially when the size of the problem increases.

### 3.1.3 LFT modeling of the beam mass

Modeling the mass of the beam ( $m_b$ ) uncertain in LFT, is not trivial. Namely, the beam mass occurs as square root in the modal matrix (see section 2.2). Because of that, we rewrite the uncertainty of  $m_b$  in the maximal and minimal deviation of the square root. From a nominal value of the beam mass of 7[kg] and a deviation of 5%, this result in:

$$m_{b,sqrt}^+ = \sqrt{7 \times 1.05}$$

$$m_{b,sqrt}^- = \sqrt{7 \times 0.95}$$

From this  $m_{b,sqrt}$  minimal and maximum we can than again define a nominal and deviation and write this variable in a LFT form. To calculate  $m$  we simply multiply  $m_{sqrt}$  with itself.

### 3.1.4 LFT modeling of total plant

Now that all the uncertainty parameters are brought to the LFT form using the standard operations, it is possible to bring the whole analytical model of the spacecraft in LFT. This is implemented in a Matlab environment, where a number of variables can be modified and the LFT of the total plant is calculated automatically. The input variables that can be adjusted are summed up in table3.2.

Input variables
number of beams
number of modes
if $\omega$ is uncertain
if $\xi$ is uncertain
if mass beam is uncertain
if spacecraft mass is uncertain
if spacecraft inertia is uncertain

Table 3.2: Input variables in Matlab script

If we would model the total plant with 6 beams, 2 number of modes for each beam and all parameters uncertain, than the total size of the  $\Delta$ -block will be  $246 \times 246$ . Using (balanced) model reduction techniques as mentioned before, this can be reduced to a size of the  $\Delta$ -block of  $138 \times 138$ .

## 3.2 Rearrange the $\Delta$ -block

If we look al bit closer to one of the applied standard operations on LFTs, we see that the  $\Delta$ -block extends when adding more uncertainty parameters to model the plant. The problem that arises here, is that the resulting  $\Delta$ -block is not sorted anymore. This is already shown in equation (3.3) were combining the LFTs of two uncertain pulsations and damping in the  $Y$  and  $Z$ -direction results in a  $\Delta$ :

$$\Delta = \begin{bmatrix} \delta_1 & 0 & 0 & 0 & 0 & 0 \\ 0 & \delta_2 & 0 & 0 & 0 & 0 \\ 0 & 0 & \delta_1 & 0 & 0 & 0 \\ 0 & 0 & 0 & \delta_2 & 0 & 0 \\ 0 & 0 & 0 & 0 & \delta_3 & 0 \\ 0 & 0 & 0 & 0 & 0 & \delta_4 \end{bmatrix} \quad (3.4)$$

In order to start a  $\mu$ -analysis on a LFT, the above  $\Delta$ -block must be rearranged in such a way that in the end all the same  $\delta$ 's follows each other on the diagonal. In other words, they can be combined in one  $\delta$  multiplied with  $I$  and the size of  $I$  is equal to the number of occurrence of the specific  $\delta$ . This sorting is achieved by pre and post multiplication of the  $\Delta$  with permutation matrix  $P$  and it's transposed, where:

$$\tilde{\Delta} = P\Delta P^T$$

Note that  $P^T = P^{-1}$  due to the fact that  $P$  is a permutation matrix. In the case of equation 3.4 the used  $P$  that sorts the  $\Delta$  is:

$$P = \begin{bmatrix} 1 & 0 & 0 & 0 & 0 & 0 \\ 0 & 0 & 1 & 0 & 0 & 0 \\ 0 & 1 & 0 & 0 & 0 & 0 \\ 0 & 0 & 0 & 1 & 0 & 0 \\ 0 & 0 & 0 & 0 & 1 & 0 \\ 0 & 0 & 0 & 0 & 0 & 1 \end{bmatrix}$$

Each column of the matrix  $P$  is linked to the  $\delta$  on the same column of the  $\Delta$ . The row of the  $P$  where the 1 is placed is then corresponding to the location on the diagonal of the  $\Delta$  where the  $\delta$  should be placed. This sorting of the  $\Delta$  and thus the defining of the  $P$  is also automated using Matlab.

### 3.3 Verification of LFT model

To verify whether the obtained LFT is correct, the LFT and the model of the satellite as described in [2] are determined and compared in a Bode diagram. Thus first the LFT is calculated with 6 beams and 2 pulsations for each beam. Then the upper LFT is derived, where each  $\delta$  of the  $\Delta$ -block is replaced with a numerical value according to:

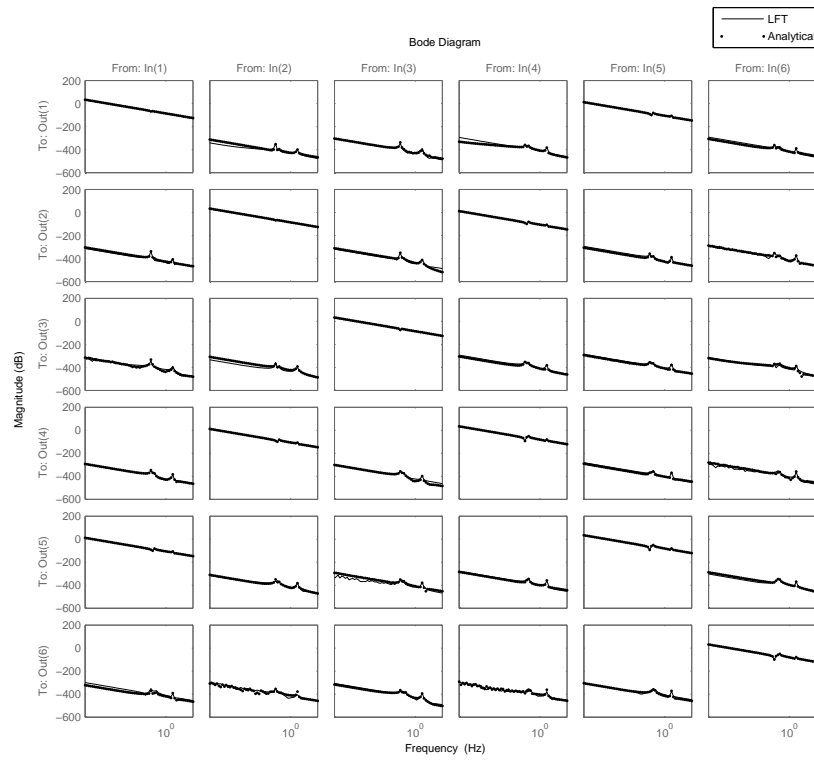
$$\delta = \frac{p - \bar{p}}{p_\delta}$$

Thus if we're interested in the satellites nominal model, all the  $\delta$ 's are replaced with 0 and the upper LFT is derived. In this way, two models are compared: one of the satellites nominal plant and one deviated plant. In the last plant the satellite mass and inertia is chosen 515.32 and 241.76 respectively and all the beam uncertain parameters are replaced according to table 3.3.

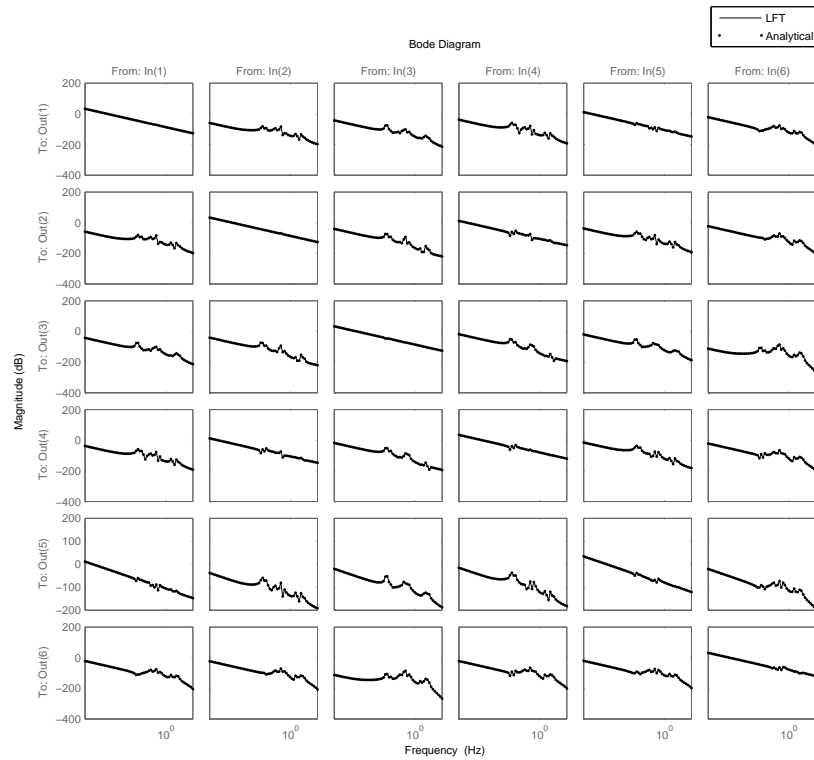
Beam #	Frequency along Ybeam axis (Hz)	Frequency along Zbeam axis (Hz)	Damping along Ybeam axis (%)	Damping along Ybeam axis (%)	Beam mass
1	0,3918	0,4979	0,9928	0,4199	7.2051
2	0,3578	0,0993	0,6704	0,1074	6.7293
3	0,4650	0,0774	0,1151	0,2956	7.3392
4	0,4856	0,3648	0,5640	0,4578	7.1562
5	0,2492	0,1011	0,4647	0,9748	6.8960
6	0,3938	0,0861	0,3239	0,6845	6.6621

Table 3.3: Different parameters for each beam

The result is shown in figure 3.3. In the case of the nominal plant, we can see very small differences between the two models. These differences occur at about  $-400[dB]$  and are dedicated to rounding errors. From these Bode diagrams we conclude that the LFT represents the right system.



(a) Nominal plants



(b) Perturbed plants

Figure 3.3: Compare Bode of satellite plant and satellite LFT

# Chapter 4

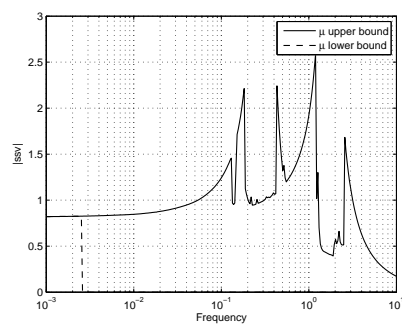
## $\mu$ -analysis

In the previous chapter, the uncertainty modeling of the satellite is performed using LFT modeling techniques. The bode diagram of the MIMO QFT controller is shown in appendix C. In this chapter the  $\mu$ -analysis is discussed. The applied software to calculate the bounds on  $\mu$ , is motivated in Appendix B. Due to some numerical pitfalls some tradeoffs are made between the number of uncertain parameters and the accuracy of the bound calculation, to control the calculation time. The  $\mu$ -analysis of the total plant with all parameters uncertain is therefor not performed and other analyses are applied to gain more insight in the robust stability of the plant in combination with the MIMO QFT controller.

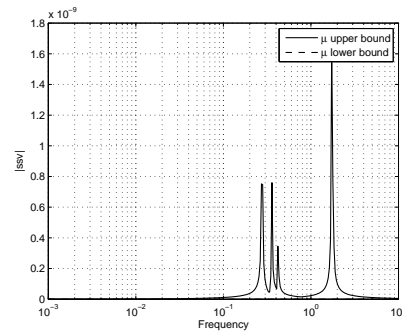
### 4.1 $\mu$ -analysis of al parameters separately

In this first section we analyze the influence of all parameters using the  $\mu$  analysis. From this we should get a better picture of which parameter is the most critical for robust stability. In figure 4.1 the  $\mu$ -analysis of all the parameters separately are plotted for 1 beam taken as uncertain and the others 5 nominal. If we look closely to the figures, we notice two things. One, as mentioned in Appendix B the algorithm leaves room to adjust the accuracy of the  $\mu$  computation. Because we investigate small  $\Delta$ -blocks, the  $\mu$ -analysis is performed crude. This is the reason why the  $\mu$  seems to be larger than 1 for the case of the pulsation uncertain, while it's actual not. Two, the lower bound is for almost all frequencies equal to zero. This is due to the convergence problem of the algorithm.

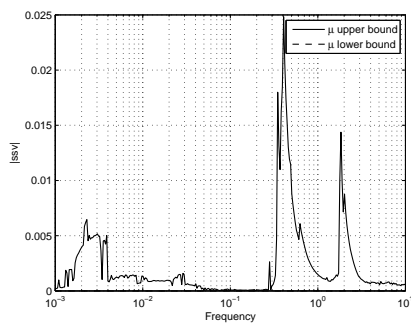
From these figures we conclude that the pulsation has the worst influence on the  $\mu$ . Thus the logical thing to do now is to model the satellite with only the pulsation uncertainty.



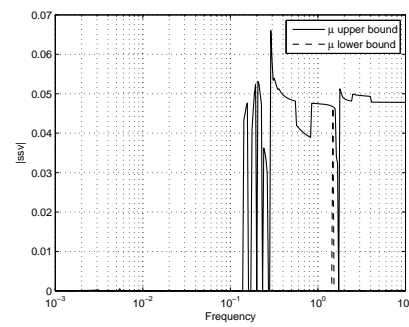
(a) pulsation uncertain



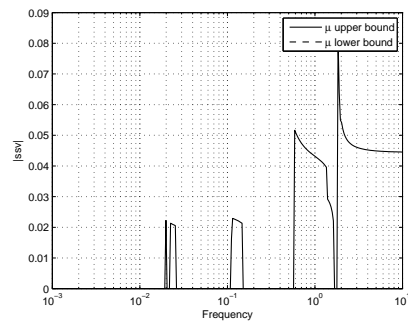
(b) damping uncertain



(c) beam mass uncertain



(d) spacecraft mass uncertain



(e) spacecraft inertia uncertain

Figure 4.1: Compare  $\mu$ -analysis of one beam and different parameters uncertain.

## 4.2 Model satellite with pulsation uncertain

Modeling the satellite with only the pulsation uncertain results in a  $M\Delta$  structure with:

$$\Delta = \begin{bmatrix} \delta_1 I_{4 \times 4} & 0 & 0 & 0 & 0 & 0 & 0 & 0 & 0 & 0 & 0 & 0 \\ 0 & \delta_2 I_{4 \times 4} & 0 & 0 & 0 & 0 & 0 & 0 & 0 & 0 & 0 & 0 \\ & & & & \vdots & & & & & & & \\ 0 & 0 & 0 & 0 & 0 & 0 & 0 & 0 & 0 & 0 & 0 & \delta_{12} I_{4 \times 4} \end{bmatrix}$$

Here  $\delta_1$  is representing the uncertainty of  $\omega_Y$  of beam 1, the second delta ( $\delta_2$ ) belongs to  $\omega_Z$  of beam one and the third delta represents  $\omega_Y$  of beam 2, etcetera. This  $\Delta$  already causes computation problems (reduction techniques did not reduce the size of  $\Delta$  enough) and therefore the beam is modeled with only one mode for each beam. This reduces the size of the  $\Delta$ -block by half and the resulting block looks like:

$$\Delta = \begin{bmatrix} \delta_1 I_{2 \times 2} & 0 & 0 & 0 & 0 & 0 & 0 & 0 & 0 & 0 & 0 & 0 \\ 0 & \delta_2 I_{2 \times 2} & 0 & 0 & 0 & 0 & 0 & 0 & 0 & 0 & 0 & 0 \\ & & & & \vdots & & & & & & & \\ 0 & 0 & 0 & 0 & 0 & 0 & 0 & 0 & 0 & 0 & 0 & \delta_{12} I_{2 \times 2} \end{bmatrix}$$

So now we can perform a  $\mu$ -analysis with only one pulsation modeled uncertain for each beam.

## 4.3 $\mu$ -analysis pulsation uncertain

The previously mentioned  $M\Delta$  structure is used to calculate the bounds on  $\mu$ . Because this  $\Delta$  is pretty large, the algorithm encounters less numerical problems and therefore the bounds on  $\mu$  are tightened. Hence, we expect the resulting upper bound is seriously approaching the  $\mu$ . See figure 4.2 for the bounds on  $\mu$ .

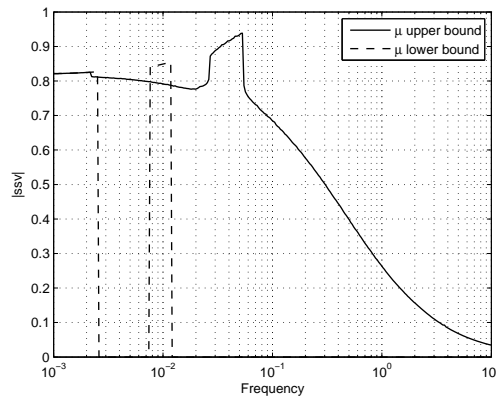


Figure 4.2:  $\mu$ -analysis with 6 beams uncertain and number of modes is 1 for each beam.

From this figure we conclude that the system seems robustly stable. As mentioned before, the lower bound does not converge and thus a solution has to be used to find a worst case  $\Delta$ .

## 4.4 Worst case $\Delta$ for pulsation uncertain

By adding a small complex perturbation, scaled with a factor  $\alpha$  (see appendix B), the lower bound of the  $\mu$  converges and a worst case  $\Delta$  is computed. In figure 4.3 we see the  $\mu$ -analysis of the new uncertain system, with different scaling of the added complex perturbations, i.e. different  $\alpha$ 's. To keep the calculation time short, in this case only the first three beams are considered uncertain with one pulsation uncertain each beam (the other 3 beams are thus modeled as the constant nominal values =  $0.275[Hz]$ ).

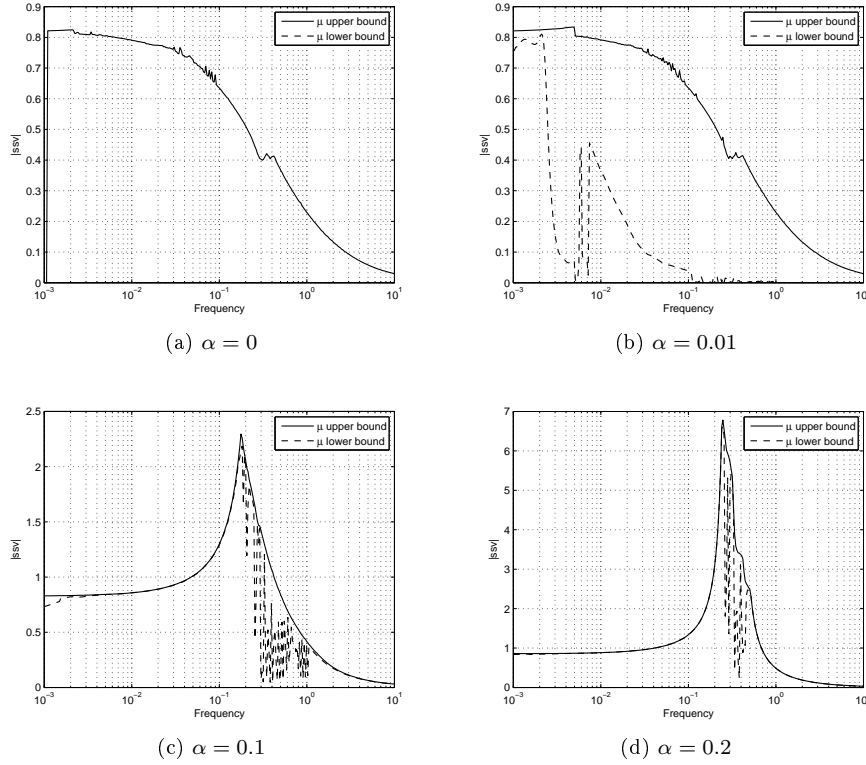


Figure 4.3: Compare mixed  $\mu$  with differed values of  $\alpha$ .

From these figures we suggest that choosing  $\alpha = 0.1$  would do, because this results in a converging lower bound close to the upper bound in the worst frequencies. So now the model is again formed, with this time all 6 beams considered uncertain and still one pulsation for each beam. The resulting  $\mu$  is plotted in figure 4.4, with the  $\alpha$  chosen as 0.1.

We now can gather the  $\Delta_{wc}$  for the frequency of  $0.0516[Hz]$  (is the worst case frequency of this plant without a complex  $\Delta$  added, see figure 4.2) and we find:

$$\Delta_{wc} = -0.9833I_{24 \times 24}$$

Note that the complex part of this  $\Delta$  is neglected. From the LFT between this  $\Delta$  and the  $\omega$ 's we conclude that the worst case  $\omega$  is  $0.275 - 0.9833 \cdot 0.225 = 0.05376[Hz]$  which lies close to the frequency of  $0.0516[Hz]$ .



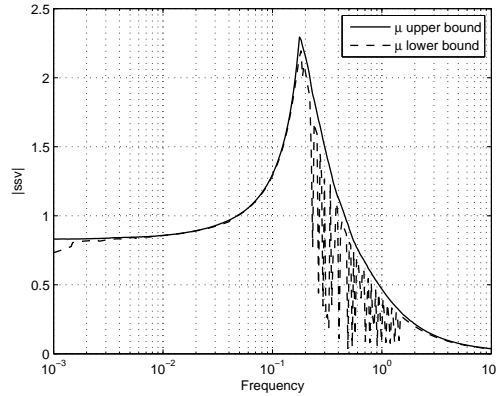


Figure 4.4:  $\mu$ -analysis with 6 beams uncertain and number of modes is 1 for each beam,  $\alpha = 0.1$ .

## 4.5 Time domain plot of pulsation worst case

Now the linear fractional transformation between the uncertainty plant (modeled with 1 mode for each beam) and the worst case  $\Delta_{wc}$  for the pulsations are computed and analyzed in the time domain. From the poles of the plant we immediately conclude that the system is unstable, because some of the poles lie in the RHP:

$$\begin{aligned} &1.270e - 004 \pm i2.540e - 001 \\ &2.032e - 004 \pm i2.540e - 001 \\ &1.778e - 004 \pm i2.540e - 001 \end{aligned}$$

But when analyzing this system in time domain, the step response simply seems to be stable, see figure 4.5. This is in principle what we would expect. Because when we look at the upper bound of  $\mu$  of this system (figure 4.2) it remains under 1 and thus this plant should be robustly stable. We expect that numerical problems are responsible for this.

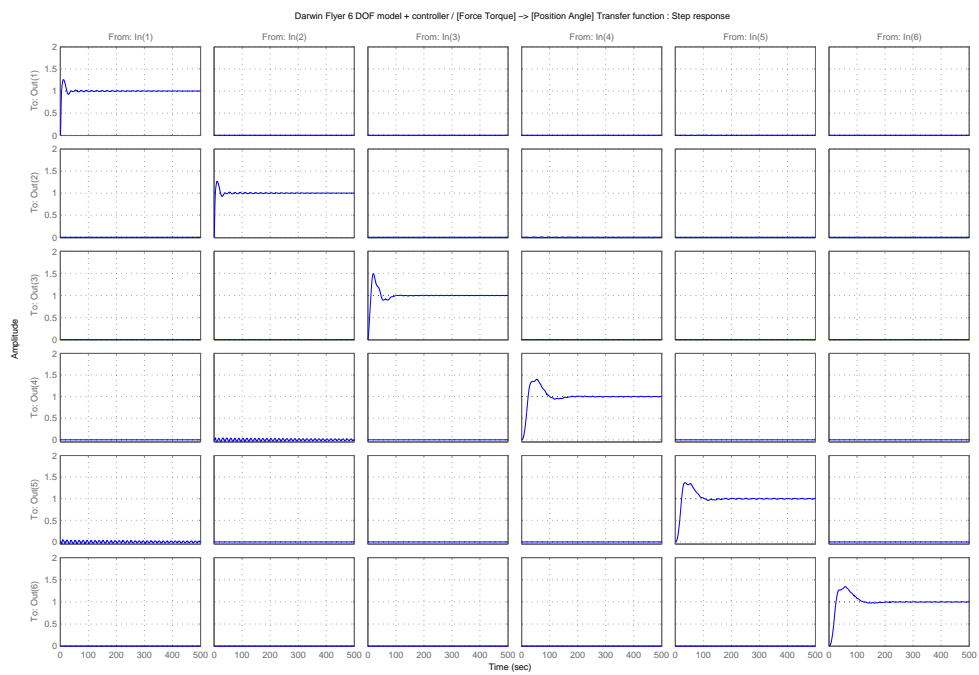


Figure 4.5: Step response of worst case plant with 1 mode for each beam.

## 4.6 Symmetric property of satellite plant

Another way to investigate the worst case  $\Delta$  for the total plant, without using the LFT of the total model is to use the symmetric property of the plant. In figure 4.6 the plant is modeled with 1 beam uncertain. Each time the number of modes for all beams are equal to 2 and the parameters that are considered uncertain are the pulsation and the damping.

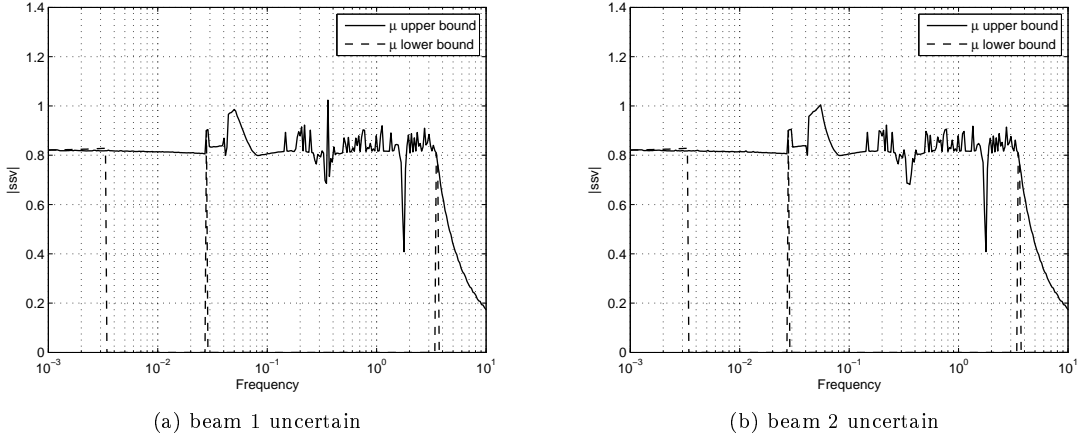


Figure 4.6: Model pulsation and damping uncertain of one beams.

The differences between the figures is the beam that is modeled uncertain. In principle it should not matter which of the 6 beams is modeled uncertain, but due to numerical issues, we see small differences between the two  $\mu$ -analysis. The main attention will go out to the frequency region around  $0.05[Hz]$ , because here both analysis are approximately the same. The main idea now is that if we would model beam 1 and 2 uncertain and thus combine the two uncertainties, then will the resulting  $\mu$  still be the largest around the  $0.05[Hz]$ ? In other words, is it possible to gain insight in the  $\mu$  of the total plant by just considering one beam uncertain?



# Chapter 5

## Conclusion

In this report the uncertainty modeling of the Darwin type spacecraft is achieved, using LFT modeling. This LFT model was ready to be used for  $\mu$ -analysis purpose, but when applying this  $\mu$  several problems occurred. The main two issues were:

- Calculation time
- Convergence problems of lower bound

To overcome these problems some measures are described. The first is to reduce the size of the LFT by analyzing the influence of all uncertainty parameters separately and to focus the  $\mu$ -analysis on the uncertainty with the most influence on  $\mu$ . The second measure was to apply a fix to overcome the convergence problem of the lower bound.

The first measure leads to the conclusion that the pulsations are the most critical parameters of the model. This is concluded from the analysis of one beam uncertain and by reducing the  $\Delta$  block of the total uncertain plant. From this conclusion the whole plant was again modeled, but now only with the pulsations uncertain. This led to a LFT model with a smaller block, from which a worst case  $\Delta$  is calculated.

To obtain the worst case  $\Delta$ , the fix was applied on the problem. By adding a small complex  $\Delta$  to the real  $\Delta$ , the lower bound converged and the worst case  $\Delta$  was computed at the worst frequency ( $= 0.0516[Hz]$ ):

$$\Delta_{wc} = -0.9833I_{24}$$

It is questionable if adding a small complex part and afterward neglecting it, is not affecting the reliability of the calculated worst case  $\Delta$ . In this particular case, it seems that it does not. Because first of all, the upper bound of the LFT with and without the complex added at the frequency of  $0.0516[Hz]$  seems to be almost the same. Secondly, if we would compute the worst  $\omega$  from this  $\Delta_{wc}$ , it is  $0.05376[Hz]$ . This is close to the critical frequency of  $0.0516[Hz]$  and this is comparable.

From the results we can conclude that the worst case  $\Delta$  is capable to make the plant unstable or that we have numerical problems in the plant. We conclude this by calculating the poles of the worst case plant. On the other hand, if we observe the step response of this worst case plant, the output is bounded and this implies a stable system. We therefore conclude that the observable and controllable poles are stable, but the system is not internally stable.

## Recommendations

The combination between the used  $\mu$  software and the large real valued parametric  $\Delta$  of the plant results in computational problems. This problem might be overcome by using other  $\mu$  software or by modeling the uncertainty differently. This last suggestion can be done by modeling the uncertainty according to a method described in [4]. This boils down to capturing all uncertainties in a weight filter. The advantage is that multiple sources of uncertainty can be modeled with less complex  $\delta$ 's. The disadvantage of this method is that the uncertainty parameters must be gridded when defining the weight filters. Naturally it is possible that the worst case plant is formed when choosing the parameters between the grids and thus that the obtained weight filters give optimistic results. The risk of this gridding might be decreased when using the results of this report, namely take a higher grid density around the critical frequency and for the pulsations. Another disadvantage of this method is that because the parametric uncertainty is combined and represented by less complex  $\delta$ 's, the worst case plant cannot be obtained from this method.

# Appendix A

## Standard operations on LFTs

The standard operations on LFTs used in this document are summed up in this appendix. These operations are adapted from [3]. In this appendix the following LFT systems are used:  $\mathcal{F}_u(M, \Delta)$ ,  $\mathcal{F}_u(M', \Delta')$  and  $\mathcal{F}_u(M'', \Delta'')$ , where

$$M = \left[ \begin{array}{cc|c} M_{11} & M_{12} & \\ \hline M_{21} & M_{22} & \end{array} \right]; M' = \left[ \begin{array}{cc|c} M'_{11} & M'_{12} & \\ \hline M'_{21} & M'_{22} & \end{array} \right]; M'' = \left[ \begin{array}{cc|c} M''_{11} & M''_{12} & \\ \hline M''_{21} & M''_{22} & \end{array} \right]$$

### Transposition

$$\mathcal{F}_u(M, \Delta)^T = \mathcal{F}_u \left( \left[ \begin{array}{cc|c} M_{11}^T & M_{12}^T & \\ \hline M_{21}^T & M_{22}^T & \end{array} \right], \Delta \right)$$

Note the restriction is, that  $\Delta = \Delta^T$ .

### Addition

$$\mathcal{F}_u(M', \Delta') + \mathcal{F}_u(M'', \Delta'') = \mathcal{F}_u \left( \left[ \begin{array}{cc|c} M'_{11} & 0 & M'_{12} \\ \hline 0 & M''_{11} & M''_{12} \\ \hline M'_{21} & M''_{21} & M'_{22} + M''_{22} \end{array} \right], \left[ \begin{array}{cc} \Delta' & 0 \\ 0 & \Delta'' \end{array} \right] \right)$$

### Multiplication

Between LFT objects:

$$\mathcal{F}_u(M', \Delta') \mathcal{F}_u(M'', \Delta'') = \mathcal{F}_u \left( \left[ \begin{array}{cc|c} M'_{11} & M'_{12} M''_{21} & M'_{12} M''_{22} \\ \hline 0 & M''_{11} & M''_{12} \\ \hline M'_{21} & M'_{22} M''_{21} & M'_{22} M''_{22} \end{array} \right], \left[ \begin{array}{cc} \Delta' & 0 \\ 0 & \Delta'' \end{array} \right] \right)$$

Between LFT and constant matrix  $A$  (pre-multiplication):

$$A \mathcal{F}_u(M, \Delta) = \mathcal{F}_u \left( \left[ \begin{array}{cc|c} M_{11} & M_{12} & \\ \hline A & M_{21} & A & M_{22} \end{array} \right], \Delta \right)$$

(post-multiplication)

$$\mathcal{F}_u(M, \Delta) A = \mathcal{F}_u \left( \left[ \begin{array}{c|c} M_{11} & M_{12} A \\ \hline M_{21} & M_{22} A \end{array} \right], \Delta \right)$$

## Concatenation

Horizontal:

$$[ \mathcal{F}_u(M', \Delta') \quad \mathcal{F}_u(M'', \Delta'') ] = \mathcal{F}_u \left( \left[ \begin{array}{cc|cc} M'_{11} & 0 & M'_{12} & 0 \\ 0 & M''_{11} & 0 & M''_{12} \\ \hline M'_{21} & M''_{21} & M'_{22} & M''_{22} \end{array} \right], \left[ \begin{array}{cc} \Delta' & 0 \\ 0 & \Delta'' \end{array} \right] \right)$$

Vertical:

$$\left[ \begin{array}{c} \mathcal{F}_u(M', \Delta') \\ \mathcal{F}_u(M'', \Delta'') \end{array} \right] = \mathcal{F}_u \left( \left[ \begin{array}{cc|c} M'_{11} & 0 & M'_{12} \\ 0 & M''_{11} & M''_{12} \\ \hline M'_{21} & 0 & M'_{22} \\ 0 & M''_{21} & M''_{22} \end{array} \right], \left[ \begin{array}{cc} \Delta' & 0 \\ 0 & \Delta'' \end{array} \right] \right)$$

## Juxtaposition

$$\left[ \begin{array}{cc} \mathcal{F}_u(M', \Delta') & 0 \\ 0 & \mathcal{F}_u(M'', \Delta'') \end{array} \right] = \mathcal{F}_u \left( \left[ \begin{array}{cc|cc} M'_{11} & 0 & M'_{12} & 0 \\ 0 & M''_{11} & 0 & M''_{12} \\ \hline M'_{21} & 0 & M'_{22} & 0 \\ 0 & M''_{21} & 0 & M''_{22} \end{array} \right], \left[ \begin{array}{cc} \Delta' & 0 \\ 0 & \Delta'' \end{array} \right] \right)$$

## Inversion

It is assumed that  $M_{22}$  is invertible.

$$\mathcal{F}_u(M, \Delta)^{-1} = \mathcal{F}_u \left( \left[ \begin{array}{c|c} M_{11} - M_{12}M_{22}^{-1}M_{21} & M_{12}M_{22}^{-1} \\ \hline -M_{22}^{-1}M_{21} & M_{22}^{-1} \end{array} \right], \Delta \right)$$

## Rearrange $\Delta$

Rearrange the  $\Delta$  using permutation matrix  $P$  (thus  $P^{-1} = P^T$ )

$$\mathcal{F}_u(\tilde{M}, \tilde{\Delta}) = \left( \left[ \begin{array}{c|c} PM_{11}P^T & PM_{12} \\ \hline M_{21}P^T & M_{22} \end{array} \right], P\Delta P^T \right)$$



# Appendix B

## mussv algorithm

This appendix is dedicated to the in this report used  $\mu$  algorithm. The algorithm and the associated Matlab commando is clarified. We will not go into depth whit this, but only note the calculation routines shortly, to make the origin of the arisen problems clearer. Also the Matlab commando will be treated roughly, were only the input and output of this commando that is relative for this report will be discussed. For more detailed information on the `mussv`, the reader is referred to [1]. After this, the problems when using this tool in practice and options to tackle these problems will be discussed.

### Computing bounds on $\mu$

One problem of the  $\mu$ -analysis is that the exact derivation of  $\mu$  is most of the time practically impossible. Fortunately there are some routines available which approximate the value of  $\mu$ . The approximation used in this report is adapted from Matlabs Robust Control Toolbox and goes by the name `mussv`.

In this routine an upper and lower bound on  $\mu$  is derived. So this boils down to:

$$bnd_{lower} \leq \mu(M) \leq bnd_{upper} \tag{B.1}$$

#### Lower bound

Here the software uses a power algorithm (iteration) for computation of the lower bound to search for the smallest  $\Delta$  which makes  $\det(I - M\Delta) = 0$ . But because the algorithm isn't convex, the resulting  $\mu$  might be to small (cause the algorithm converges to a local maximum in stead of the global maximum). Especially when the  $\Delta$  consist of purely real uncertainties, it even can lead to no convergence at all.

## Upper bound

To find the upper bound of  $\mu$ , the following routine is used:

If there is a  $\beta > 0$  such that

$$\bar{\sigma} \left[ (I + G_l^2)^{-\frac{1}{4}} \left( \frac{1}{\beta} D_l M D_r^{-1} - j G_m \right) (I + G_r^2)^{-\frac{1}{4}} \right] \leq 1 \quad (\text{B.2})$$

then

$$\mu_{\Delta}(M) \leq \beta$$

The  $G$  and  $D$  matrices are scaling matrices with predefined structure. See [1] for more detailed information. Although this routine to approximate the upper bound might be too conservative, it is a convex problem and thus leads to a solution, even if the perturbations are purely real.

In Matlab the `mussv` commando is called as shown below:

```
[Bounds, MuInfo] = mussv(M, blk, options)
```

The resulting upper and lower bound of  $\mu$  is stored in the variables `Bounds`, while the `MuInfo` stores additional information like the worst case  $\Delta$ 's and some variables to verify the correctness of the computed bounds. The `M` matrix in combination with `blk` forms the uncertainty system under investigation. In the last input variable 'options' the user is able to adjust some options. Although these adjustments are optional, we will highlight one option here, because its functionality turned out to be useful. In the standard case, the applied  $\mu$  analysis is done roughly. For relative small  $\mu$  problems this results in a fast and accurate calculation of the bounds. When the size of the  $\Delta$  block (and thus the size of the  $\mu$  problem) increases the calculated bounds get more inaccurate. However it is possible to tighten the bounds on  $\mu$  to get more realistic bounds. This is done by changing the options parameter. For example, set options to 'c' to tighten the bounds. Set it to 'C1' for an even greater accuracy. The greatest accuracy is obtained by setting options to 'C9'. Naturally there is a disadvantage when increasing the accuracy, cause calculation time will increase also. Furthermore one restriction on the accuracy increasing is noted, cause analyzing small  $\mu$  problems with high accuracy can lead to numerical problems.

## Problems with $\mu$ bounds calculations

When calculating the bounds some critical problems occur. The main two problems are the computation time and the lower bound convergence problem which is mentioned before.

### Computational time

Naturally the time it takes to compute the upper and lower bound, depends on the size of the  $\mu$  problem. The larger the size of the  $\Delta$ , the more uncertainty parameters have to be evaluated and thus the more time it takes. In addition of that, the accuracy of the bounds computation has to be increased when the size of the  $\mu$  problem increases, which results in an even more time consuming calculation.

Modeling all the parameters uncertain results in a  $M\Delta$ -structure of the plant, where the size of  $\Delta$  becomes very large ( $= 246 \times 246$ ). In other words, to model all parameters uncertain, there are 246  $\delta$ 's used and due to the fact that only real parameters are modeled, all  $\delta$ 's lie between  $(-1 \dots 1)$ . Because

the structure of the analytical model, some  $\delta$ 's occurs more than ones. The size of the  $\Delta$ -block in combination with the multiple occurrence of some  $\delta$ 's results in a very large calculation time of the upper and lower bounds of  $\mu$ . Due to this fact, the actual calculation of the upper and lower bound of the whole analytical model with all parameters considered uncertain is not performed. Unfortunately there is no fix to overcome this problem.

## Convergence problems of lower bound

The worst case  $\Delta$  cannot be obtained from the upper bound, so we need a lower bound to get the worst case plant. There is previously stated that modeling all uncertain parameters of a plant real, results in convergence problems of the lower bound. This leads to the conclusion that in the case of this report we cannot obtain a worst case  $\Delta$ . In [1] there is suggested a fix to tackle this real perturbed problem. By summing up a smaller complex perturbation with each real perturbation, the algorithm should overcome the convergence problems, see figure B.1. To give some physical meaning to this

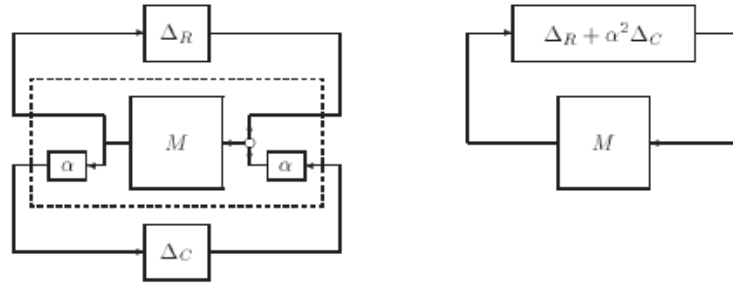


Figure B.1: Replacing Real Uncertainty with Real plus Complex Uncertainty

small complex perturbation and thus to justify such addition from engineering's point of view, the added complex perturbation can be dedicated to neglected dynamics. Naturally the size of the  $\Delta$  block increases with a factor 2, because the original real Delta-block ( $\Delta_{real}$ ) is replaced with a mixed Delta block:

$$\Delta_{mixed} = \begin{bmatrix} \Delta_{real} & 0 \\ 0 & \Delta_{complex} \end{bmatrix}$$

This is not only a problem because the calculation time will increase, but also the resulting worst case  $\Delta$  will consist of a complex part, which cannot be inserted in the original plant to analyze the effect in time domain. However, by choosing the scaling factor  $\alpha$  small, we will assume that the influence of the complex  $\Delta$  is small and therefore we will neglect this complex part, when implementing the worst case  $\Delta$  in time domain.



# Appendix C

## Bode diagram of MIMO QFT controller

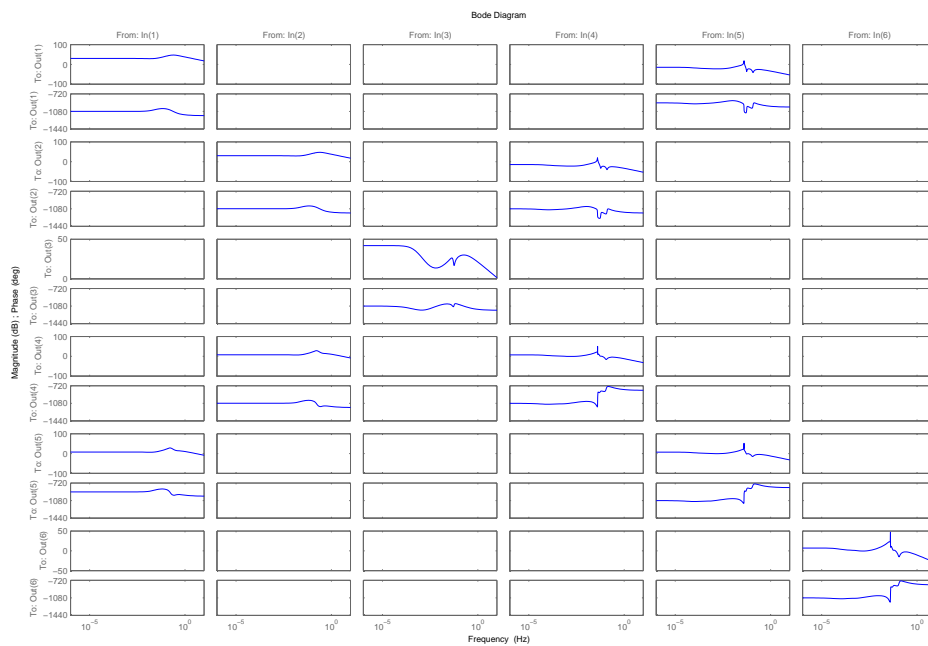


Figure C.1: Bode diagram of MIMO QFT controller



# Bibliography

- [1] Gary J. Balas, John C. Doyle, Keith Glover, Andy Packard, and Roy Smith.  *$\mu$ -Analysis and Synthesis Toolbox For Use with Matlab*. The MathWorks Inc., 1998.
- [2] G. Bodineau. Aocs for large flimsy appendages, system requirement document & aocs architecture definition. 2003.
- [3] J.-F. Magni. User manual of the linear fractionalrepresentation toolbox, version 2.0. 2006.
- [4] S. Skogestad and I. Postlethwaite. *Multivariable Feedback Control, Analysis and Design*. Wiley, 2005.
- [5] Kemin Zhou, John C. Doyle, and Keith Glover. *Robust and Optimal Control*. Prentice-Hall, 1996.